Relaxation Phenomena of Random Spin System in Itinerant Magnetic Fe_xTiS_2

Yoshiaki Hara

Relaxation Phenomena of Random Spin System in Itinerant Magnetic Fe_xTiS_2

Yoshiaki Hara

Department of Materials Science, Faculty of Science, Hiroshima University,
Higashi-Hiroshima 739, Japan

Abstract

Relaxation phenomena of zero-field-cooled isothermal remanent magnetization (IRM) and field-cooled thermoremanent magnetization (TRM) in spin-glass (SG: x = 0.20 and freezing temperature T_g = 41 K) and cluster-glass (CG: x = 1/4, T_g = 53 K) phases of intercalation compound Fe_xTiS_2 have been studied using the anomalous Hall effects over the time range 10^{-1} - 10^4 s with waiting time t_w=180 - 18,000 s at low temperatures T below $T/T_g \sim 0.7$. After an applied magnetic field is switched off, the time decay of Hall resistivity (or remanent magnetization) follows a power law of the form $\rho_H = At^{-m}$ within a limited time span, where A is a constant and m an exponent . In both IRM and TRM, the exponent m depends appreciably on the applied magnetic field intensity and temperature, for which we have obtained some universal relationship with a newly introduced quantity of "*relative relaxed magnetization*". Furthermore, the decay profiles over the wide time range, where the deviations from the power law occur, are analyzed using the existing "*domain theory*" with some modifications of the theoretical expressions. With the evaluated parameters, discussions are given for the equilibrium relaxation spectra, overlap length, and time-dependent maximum relaxation times that characterize the domain growth and the dynamic properties in this material system.

1. Introduction

Intercalation compound Fe_xTiS_2, formed by insertion of Fe atoms into van der Waals gaps of the host 1T-CdI_2 type TiS_2 crystal, is an 'itinerant' magnetic material, whose salient feature is characterized by the presence of strong hybridization among the guest Fe atoms and the neighboring host Ti and S atoms.[1] This material exhibits various magnetic phases depending on the guest Fe concentration x, such as paramagnetic ($x < 0.01$), spin-glass (SG; $0.01 \leq x \leq 0.20$), cluster-glass (CG; $0.20 < x \leq 0.40$), and ferromagnetic phases ($x > 0.40$).[2,3] In its SG and CG phases, it shows a 'cusp' or peak in the temperature dependence of static magnetization σ or ac magnetic susceptibility χ and a field cooling effect of the magnetization,[4,5] similar to various SG and CG materials. For example, Fig. 1(a) shows the temperature dependence of the field cooled (FC) and zero-field cooled (ZFC) magnetizations σ for SG measured at $H = 0.02$ T, applied parallel and perpendicular to the c-axis. For the case of H//c, the ZFC curve shows a characteristic cusp, while the FC curve has a plateau of 0.2 emu/g, followed by a paramegnetic decrease with raising temperature, indicating that the iron spins are frozen and align preferentially along to the c-axis by the FC process. On the other hand, in the field perpendicular to the c-axis, both FC and ZFC (thogh not shown here) curves have very small valuse of σ less than 0.02 emu/g without showing any cusp. Thus Fe_xTiS_2 is a very anisotropic spin-glass material with the easy axis parallel to the c-axis, quite similar to a typical Ising spin glass of $Fe_{0.5}Ti_{0.5}O_3$.[6] Figure 1(b) illustrates the ZFC and FC curves for a cluster-glass sample $Fe_{1/4}TiS_2$ at H=0.02 T for a parallel field direction (H//c). The ZFC curve shows a peak, while the FC magnetization decreases gradually from 9.6 emu/g at 4.2 K as the temperature is raised. As shown above, the field cooling effect for the SG and CG system is quite different. For these SG

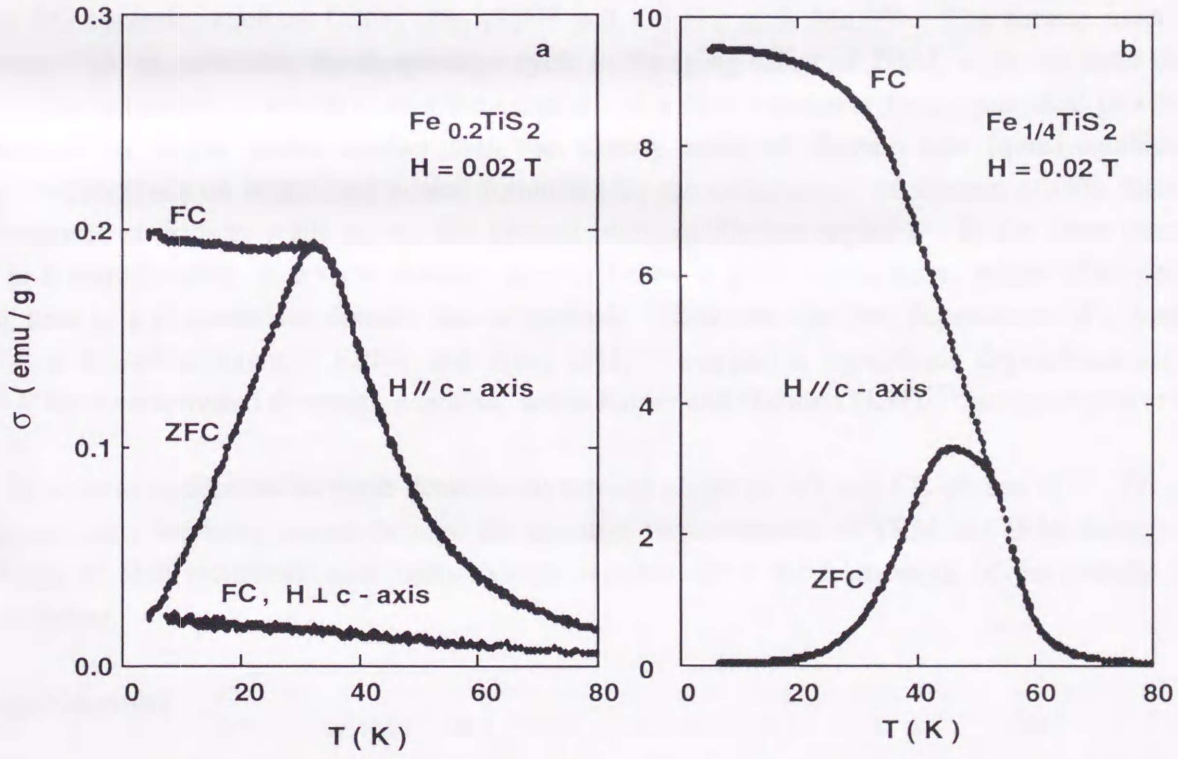

Fig. 1. (a) Field cooled (FC) and zero-field cooled (ZFC) magnetizations at $H = 0.02$ T, applied parallel and perpendicular to the c-axis, for a spin-glass sample $Fe_{0.20}TiS_2$ and (b) those for a cluster-glass sample $Fe_{1/4}TiS_2$ at $H = 0.02$ T applied parallel to the c-axis.

and CG phases of itinerant magnetic compound Fe_xTiS_2, we have studied the dynamics of zero-field-cooled isothermal remanent magnetization (IRM) and field-cooled thermoremanent magnetization (TRM) using a transport method, in contrast to magnetic measurements done for various localized systems, since this material shows an anomalous Hall effect, in which a Hall resistivity ρ_H can be expressed by the well-known form,

$$\rho_H = R_0 H + 4\pi R_s M(H), \tag{1}$$

where R_0 and R_s are the normal and extraordinary Hall coefficients, respectively, and $M(H)$ the magnetization at magnetic field H. When an applied field H is turned off, the Hall resistivity $\rho_H(t)$ is proportional to the remanent magnetization $M_r(t)$ at time t, as

$$\rho_H(t) = 4\pi R_s M_r(t). \tag{2}$$

Now with regard to the dynamical treatments of various SG systems, there are two different viewpoints. The one is the mean-field approach of Sherrington-Kirkpatrick (SK)[7] and its replica symmetry solution by Parisi[8,9], giving an infinite number of quasi-equilibrium states which are hierarchically organized in a phase space – "hierarchical kinetic model". This model has been shown to be valid for relaxation of TRM in insulating SG of Cd $Cr_{1.7}In_{0.3}S_4$[10,11] and dilute alloy Ag: Mn (Mn 2.6 at.%),[12] while from numerical and theoretical studies, Newman and Stein have pointed out that the Parisi solution to the SK model cannot apply to short-range SG.[13] The other is a phenomenological approach based on the existence of a distribution of droplets[14] or dynamical domains,[15] which has been applied to the interpretation of the aging and time decay of TRM for various SG systems, such as $CdCr_{1.7}In_{0.3}S_4$[15] and Cu (10 at.% Mn)[16]. The former model is concerned with, in particular, the temperature cycle in the aging effect of TRM, while the latter deals with its time dependence, which shows the existence of a clear crossover from dynamical processes characterized by length scales smaller than the already achieved domain size (quasi-equilibrium regime) to processes on larger time scales dominated by the continuation of domain growth through the movement of domain walls across the system (non-equilibrium regime). In the latter picture, aging is a manifestation of a slow domain growth below a glass temperature, where after certain waiting time t_w a characteristic domain size is reached. However, the time dependence of a domain size $s(t)$ is treated differently; Fisher and Huse (FH)[14] suggest a logarithmic dependence $s(t) \propto (\log t)^{1/\psi}$ from an activated dynamics scenario, while Koper and Hilhorst (KH)[15] assume a power law $s(t) \propto t^p$.

In order to understand in some detail the dynamical nature of SG and CG phases of Fe_xTiS_2, in the present study we have carried through the dynamic measurements of TRM and IRM through the time decay of Hall resitivities and discussed our results within the framework of the realistic KH domain theory.

2. Experimental

Single crystals of Fe_xTiS_2 were grown by a chemical vapor transport method;[17] the glass temperature for SG ($x = 0.20$) and CG ($x = 1/4$) is $T_g = 41$ and 53 K, respectively. Ohmic contacts to the sample with a six-probe for Hall effect measurements were made by soldering an indium metal.

The procedures of dynamical measurements are shown schematicaly in Fig. 2. For a zero-field cooled IRM measurement (solid lines), a sample was cooled at a constant rate (1 K/min) from a temperature $1.5T_g$ down to a working temperature T ($<0.7T_g$) without an external magnetic field (ZFC), followed by an application of a pulsed magnetic field H_p ($\leq$ 20 T) applied parallel to the c-axis (magnetic easy axis) of the crystal after a waiting time for t_w (=1800 s). Time decays of the Hall voltages were measured using a digital storage oscilloscope (in time range 0-50 ms) or by a nanovoltmeter (0.1-1000 s); both sample current and magnetic field directions were reversed to exclude any spurious contributions from misaligned contacts and thermoelectromotive force generated at the In/Fe_xTiS_2 interface against the Hall voltages. On the other hand, for a field-cooled TRM measurement (broken lines), the sample was cooled similarly a temperature T under a static magnetic field H_{FC}(=0.01-0.14 T). Then after a wating time t_w (=180, 1800, 18000 s), the magnetic field was switched off to zero and subsequently the time decay of TRM or the Hall voltage was recorded using the same measurement system as used for IRM measurements over the time span up to 10,000 s. After the measurements the sample was warmed up to $1.5T_g$ in zero field and then the reversed magnetic field was applied, followed by the above procedure to exclude any spurious signals.

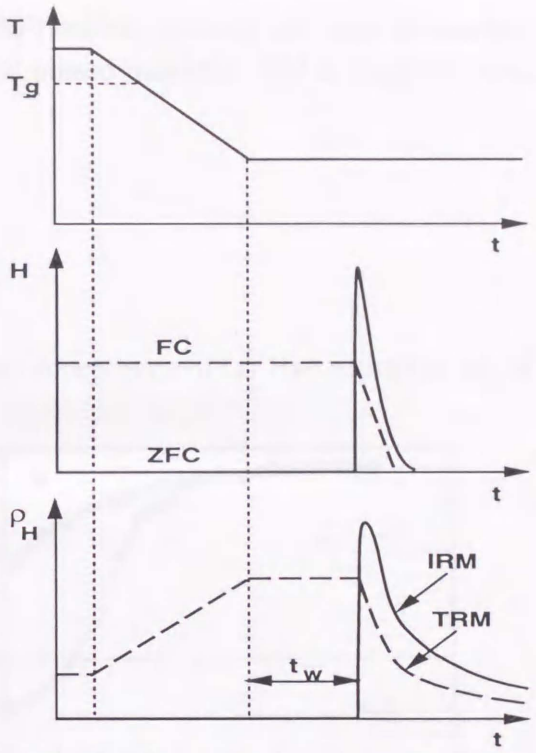

Fig. 2. Schematic measurement procedures of ZFC-IRM and FC-TRM; (a) time variation of temperature, (b) the external fields, and (c) the Hall resistivity corresponding to the magnetization of sample. Solid lines for IRM measurements and dotted lines for TRM one.

A pulsed magnetic field was produced by a home-made condenser bank system, as shown in Fig. 3, where a silicon thyristor is used for a switch, a series of electrolytic condensor banks are

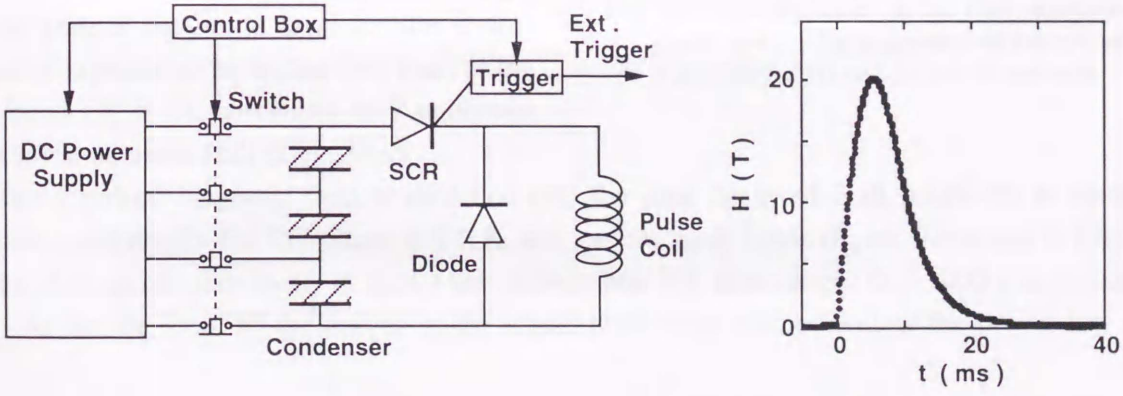

Fig. 3. (a) Schematic circuit of the system of application of pulsed magnetic fields. (b) Wave form of pulsed magnetic field used in IRM measurements, wave duration are 30-75 ms.

charged through a high dc power supply (charge capacity of 24 kJ at 1350 V), and a silicon diode is inserted parallel to a pulse coil in order to avoid the applied reversed voltage on the electrolytic condensor. The pulse magnet itself was made of a solenoidal coil of copper wires (1.5 mm in

diameter) wound around a fiber-glass reinforced plastics (FRP) bobbin; its inner and outer diameters, and length are 25, 43, and 67 mm, respectively. A typical pulsed magnetic field is depicted here, having a half-wave pulse duration of 35-70 ms.

3. Results and Discussions

3.1.1 Isothermal Remanent Magnetization (IRM)

Figure 4 shows the recorder traces of the magnetic field dependence of (a) Hall resistivity ρ_H of SG ($x = 0.20$) and (b) of CG ($x = 1/4$) at 4.2 K, respectively. These ρ_H - H curves show an appreciable hysteresis, corresponding to the magnetization curves;[4] here only the 1st and 4th quadrants of one complete cycles are depicted. After the field sweep cycle, ρ_H at $H = 0$ decays with time t, indicating the existence of a relaxation process in the transport quantity, which reflects a remanent magnetization M, as mentioned above. We see that for SG, at higher magnetic fields $H >$ 8 T well above the saturation of magnetization, the ρ_H - H curve is almost linear with H having a negative slope, similar to the CG case shown in Fig. 3(b). Using Eq.(1) and the observed magnetization curve,[4] we can estimate the values of $R_0 = -7.4 \times 10^{-9}$ and $R_s = 1.3 \times 10^{-6}$ for SG, and $R_0 = -1.2 \times 10^{-9}$ m^3/C and $R_s = 1.0 \times 10^{-6}$ m^3/C for CG at 4.2 K, respectively. These experimental results indicate that the dominant conduction carriers are electrons ($R_0 < 0$) and the density of state at the Fermi level for the down-spin band is expected to be higher than that for the up-spin band ($R_s > 0$), according to Kondorsky criterion for anomalous Hall effect.[18,19]

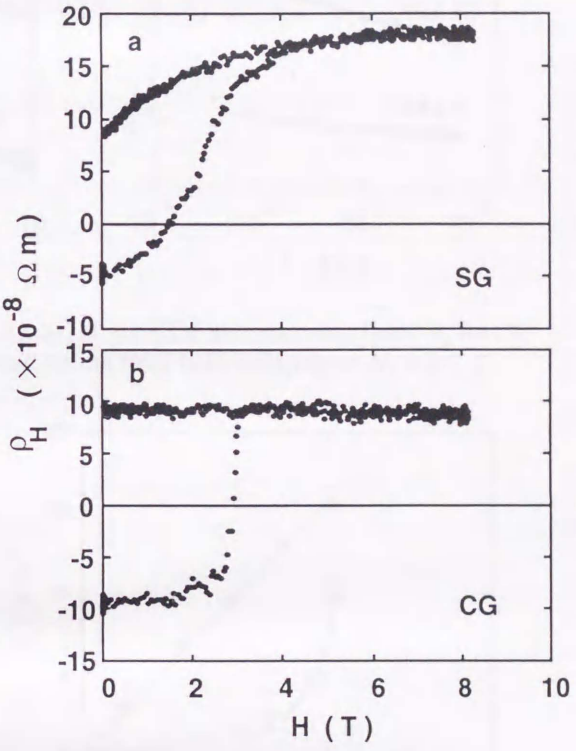

Fig. 4. Recorder traces of the Hall resistivities $\rho_H(H)$ at 4.2 K for magnetic field sweeps up to 8.2 T, (a) for SG and (b) for CG samples.

After a pulsed magnetic field is switched off, the time decay of Hall resistivity is measured. The experimental results for CG phase at 4.2 K and various peak fields H_p are illustrated in Fig. 5(a), where the Hall resistivities $\rho_H(t)$ at time t are shown over the time ranges 0.1-1000 s in logarithmic scales. As can be seen, all the curves in the whole time range studied follow the power law of the form ,

$$\rho_H(t) = A t^{-m}, \qquad (3)$$

where A is a constant and m an exponent. In Fig. 5(b) are shown similar decay curves at various temperatures over the time intervals up to 100 s for the field sweep up to $H_p = 8.2$ T. The decay

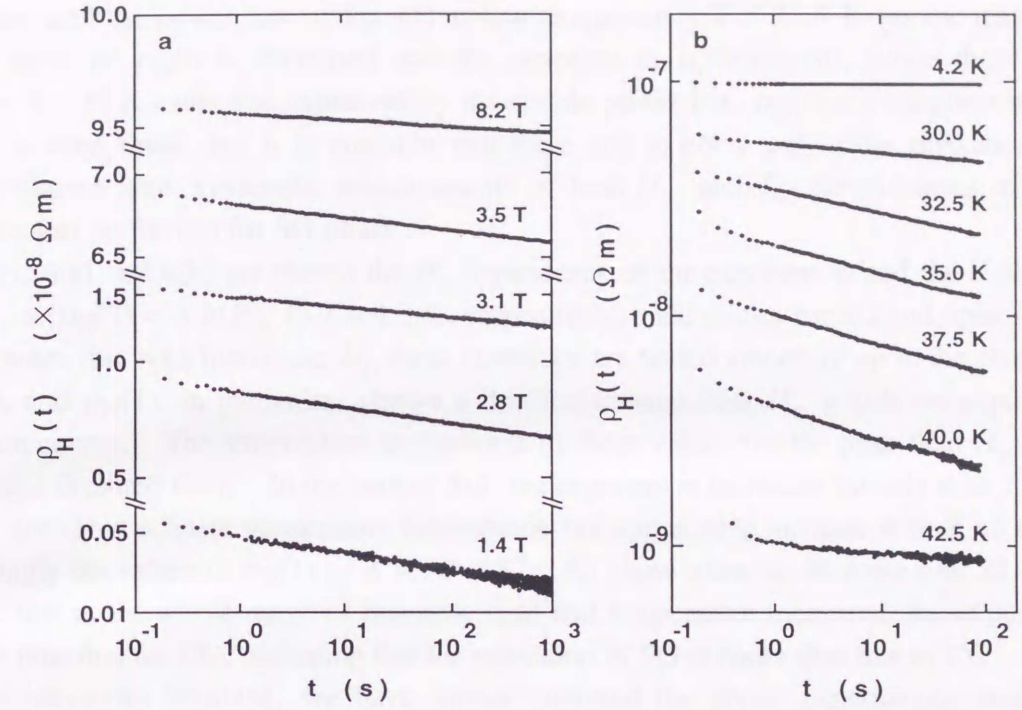

Fig. 5. (a) Time decays of the Hall resistivities $\rho_H(t)$ at 4.2 K for various sweep fields H_p for CG sample and (b) those at different temperatures for the fixed field sweep up to $H_p = 8.2$ T.

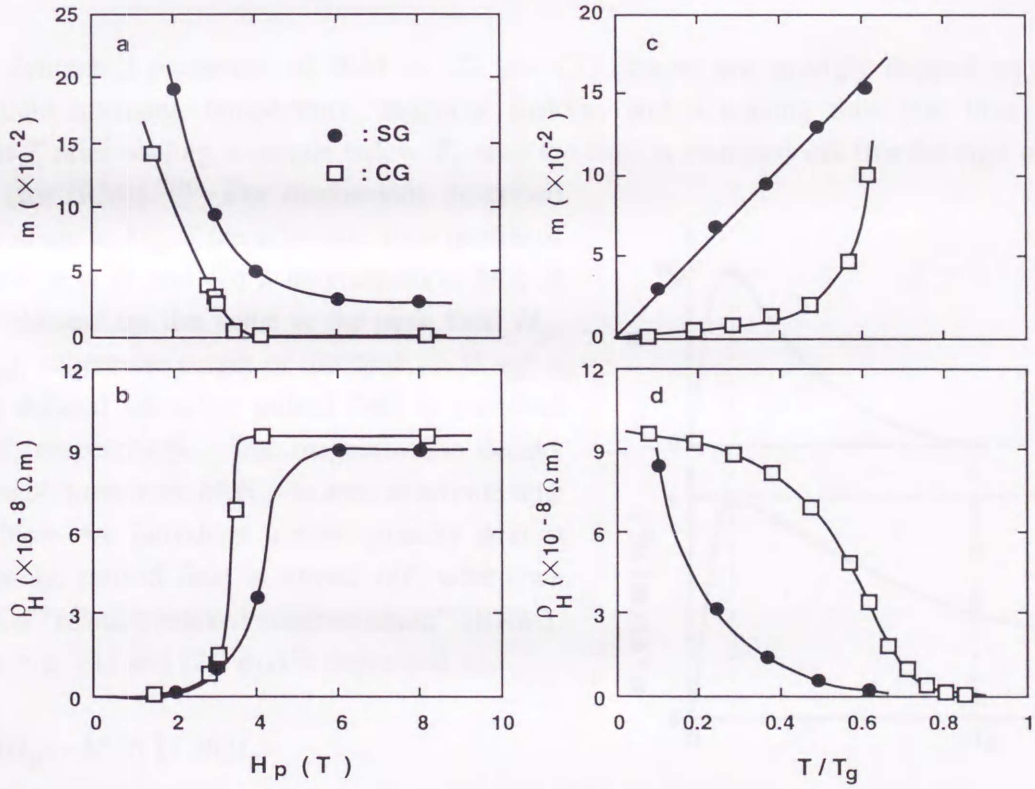

Fig. 6. (a) The values of the exponent m of SG (solid circles) and CG (open squares), (b) the Hall resistivity $\rho_H(t)$ at $t = 1$ s [$\rho_H(1) = A$] in eq. (3) at 4.2 K plotted against the peak field H_p. (c) The values of m and (d) the Hall resistivity $\rho_H(1)$ for the fixed peak field $H_p = 8.2$ T plotted against temperature; $\rho_H(1)$ for CG is equal to A at low temperatures $T \leq 32.5$ K, which does not hold at higher temperatures $T \geq 35$ K.

curves follow well the power law of Eq. (3) at low temperatures $T \leq 32.5$ K (as the temperature is raised, the value of $\rho_H(t)$ is decreased and the exponent m is increased), while those at higher temperatures $T \geq 35$ K cannot be expressed by the simple power law; $\rho_H(t)$ at the highest temperature of 42.5 K is very small, but it is apparent that there still exists a very slow relaxation process. Though not shown here, systematic measurements of both H_p- and T - dependencies of the decay profiles were also performed for SG phase.

In Figs. 6(a) and 6(b) are plotted the H_p dependence of the exponent m and the Hall resistivity $\rho_H(t)$ at $t = 1$ s [$\rho_H(1) = A$ in Eq. (3)] at 4.2 K, respectively; solid circles for SG and open squares for CG. One notes that with increasing H_p these quantities are varied smoothly up to the coercive force H_c (= 3 T), and $\rho_H(1)$, in particular, shows a drastical change near H_c, which corresponds to the magnetization curves. The temperature dependence of these values for the peak field $H_p = 8.2$ T is shown in Figs. 6(c) and 6(d). In the case of SG, the exponent m increases linearly with T, while for CG it does not show a linear temperature dependence but appreciable increase with T up to 32.5 K; correspondingly the values of $\rho_H(1)$ (= A for $T \leq 32.5$ K) show a drastic decrease near 32.5 K. We should note that in the whole range of magnetic field and temperature measured, the exponent m for SG is larger than that for CG, indicating that the relaxation of SG is faster than that of CG. To obtain any general behaviors involved, we have further analyzed the above experimental results in the following way.

3.1.2 Relative Relaxed Magnetization for IRM

The dynamical properties of IRM in SG and CG phases are strongly depend on an applied magnetic field intensity, temperature, magnetic history, and a waiting time [the time spent at a temperature T after cooling a sample below T_g until the field is switched off (for the case of TRM) or turned on (for IRM)].[20] For discussions described below, we show in Fig. 7 the schematic time profile of (a) a pulsed field H and (b) a magnetization $M(t)$ at time t, normalized by the value at the peak field H_p, $M(t)/M(H_p)$, where the origin of the time $t = 0$ and a time t_z are defined when the pulsed field is switched on and off, respectively. The magnetization decays or relaxes with time from $M(H_p)$ to zero at infinite time $t \rightarrow \infty$. Now we introduce a new quantity $\phi(t)$ at time t after the pulsed field is turned off, which we refer to as a "relative relaxed magnetization" (RRM). Then from Eqs. (1) and (2), $\phi(t)$ is expressed as,

$$\phi(t) = [M(H_p) - M_r(t)\,] / M(H_p)$$

$$= 1 - \rho_H(t) / [\rho_H(H_p) - R_0 H_p], \qquad (4)$$

where $M_r(t)$ is the remanent magnetization at time t; for simplicity, we write the value at $t = t_z$ as $\phi(t_z) = \phi$.

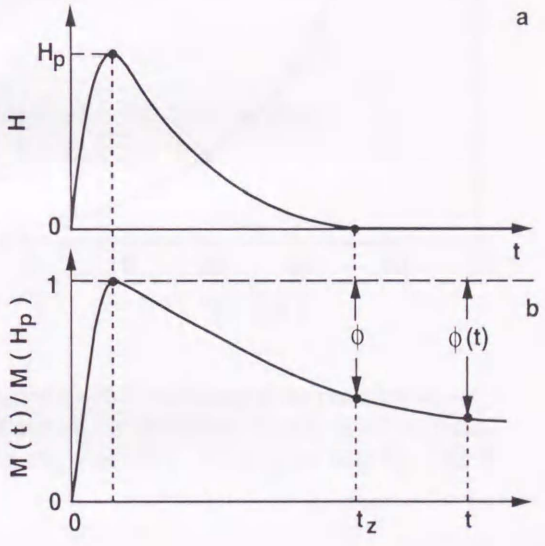

Fig. 7. Schematic time profiles of (a) the pulsed field H and (b) the magnetization $M(t)$ at time t normalized by the value at the peak field H_p, $M(t)/M(H_p)$, where the origin of the time is set when the pulsed field is switched on and time t_z is defined at pulse field H is swithced off (see text).

Figure 8(a) shows the observed values of Hall resistivities $\rho_H(t_z)$ at $t = t_z$ and $\rho_H(H_p)$ at the peak field H_p at 4.2 K plotted as a function of the peak field for CG phase. Using Eq. (4) with these values and R_0 (= -1.2×10^{-9} m^3/C), we have evaluated the values of RRM at $t = t_z$, ϕ, as depicted in Fig. 8(b), where we see that the peak field dependence of ϕ is appreciable near the coercive force H_c (= 3 T) and it becomes constant at higher fields $H_p > H_c$. The temperature dependence of the corresponding quantities for the fixed peak field H_p= 8.2 T are indicated in Figs. 8(c) and 8(d); the values of ϕ are evaluated by Eq. (4) assuming that the normal Hall coefficient R_0 is temperature independent. With increasing temperature, $\rho_H(H_p)$ is increased gradually to a constant at higher temperatures, which is considered to be due to the temperature dependent term of R_s in Eq. (1), while $\rho_H(t_z)$ is decreased; correspondingly ϕ is increased appreciably from near zero at low temperatures, approaching near unity at higher temperatures.

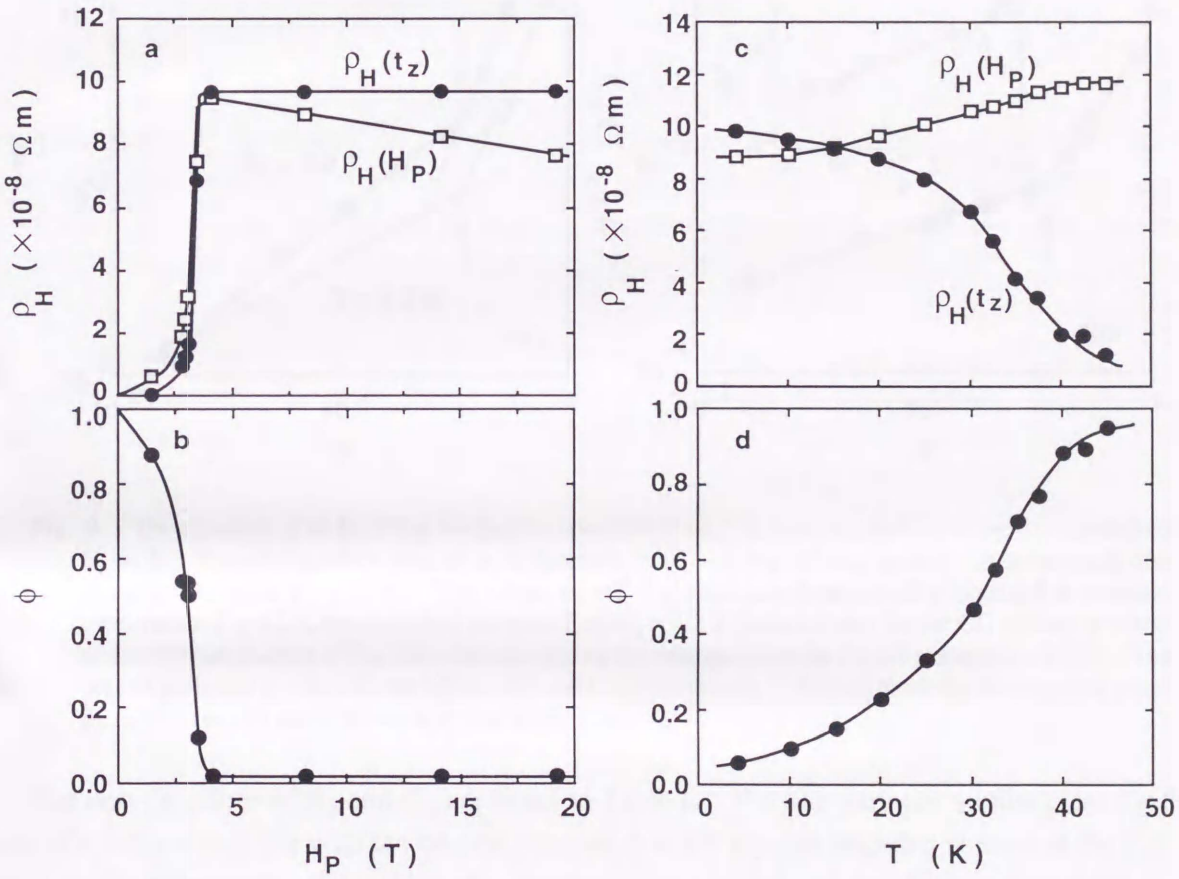

Fig. 8. (a) The values of $\rho_H(t_z)$ at $t = t_z$, $\rho_H(t_z)$ (solid circles), and the Hall resistivity at the peak field $\rho_H(H_p)$ (open squares) for CG samples and (b) the values of RRM at $t = t_z$, ϕ defined by Eq. (4), at 4.2 K plotted against the peak field H_p. (c) The values of $\rho_H(t_z)$ and $\rho_H(H_p)$, and (d) ϕ for the peak field H_p = 8.2 T plotted against temperature.

Furthermore, in order to look for a more general relation between the dynamical quantities, in Fig 9(a) we have plotted the values of m as a function of ϕ at the constant temperature 4.2 K (open circles) and at the constant peak field H_p = 8.2 T (solid circles) in logarithmic scales. In both cases, the experimental points lie well on two lines with different slopes, where the two lines cross at the common characteristic point ϕ_c = 0.34, as marked by arrows. At first sight, these two curves (solid

and open circles) are apparently different. Then in order to express the dynamical quantity m in the form of a universal function of ϕ, we have introduced a "scaled quantity" mT^{α}, as

$$mT^{\alpha} = C_i \phi^{\beta_i}, \tag{5}$$

where α and β_i are the exponents characterizing the dynamics of our CG system and C_i is a constant ($i = 1$ for $\phi < \phi_c$, $i = 2$ for $\phi > \phi_c$). Figure 9(b) illustrates the values of mT^{α} plotted against ϕ with the best-fit value of $\alpha = -1/2$ for the CG system. It is to noted that the experimental points (solid and open circles) lie well on a universal line with two different slopes β_1 for $\phi < \phi_c$ and β_2 for $\phi >$

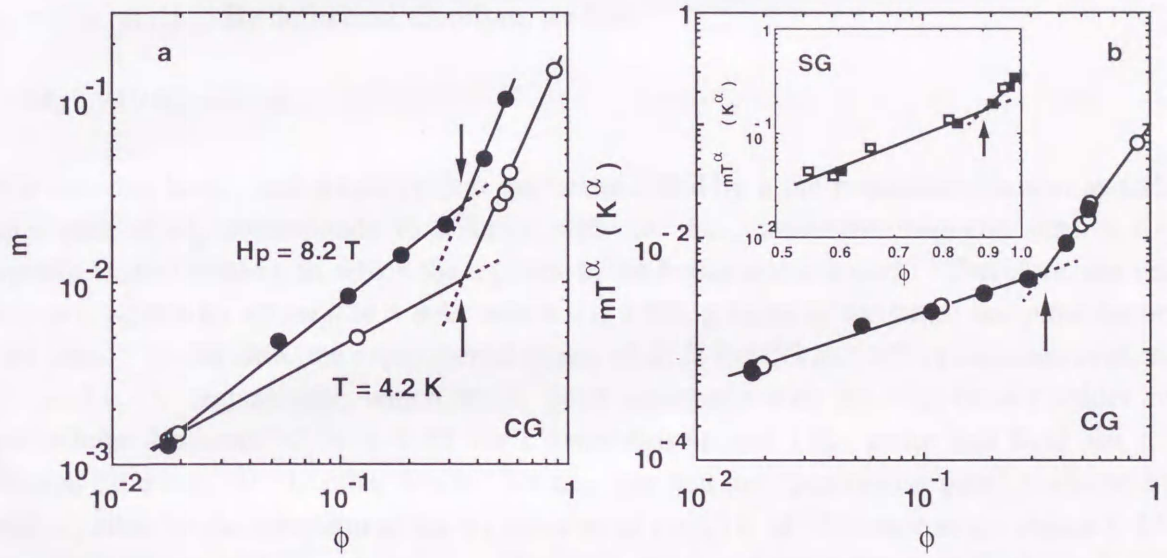

Fig. 9. The exponent m in Eq. (3) at the fixed temperature $T = 4.2$ K (open circles) and at the fixed peak field $H_p = 8.2$ T (solid circles) plotted as a function of ϕ in logarithmic scales. Arrows mark the characteristic point $\phi_c = 0.34$. The values of mT^{α} plotted as a function of ϕ obtained at constant temperature $T = 4.2$ K (open circles) and peak field $H_p = 8.2$ T (solid circles) for the CG system ($x = 1/4$) of the itinerant magnet of Fe_xTiS_2; the inset shows the enlarged plots for the SG system ($x = 0.20$). The best-fit values of α for CG and SG are -1/2 and 1/4, respectively. Arrows mark the characteristic point ϕ_c (=0.34 for CG and 0.90 for SG) (see text).

ϕ_c. The best-fit values of β_i and C_i are listed in Table I. For comparison, similar plots for the SG system (Fe_xTiS_2; $x = 0.20$) with the best-fit value of $\alpha = 1/4$ are also depicted in inset of the Fig. 9(b). In this case the expression of Eq. (5) is also satisfied with $\alpha = 1/4$ and the characteristic point of $\phi_c =$

Table I. Characteristic parameters in Eq. (5) characterizing the dynamical properties for the CG and SG systems of Fe_xTiS_2 (see text); C_i in units of K^{α}

System	α	ϕ_c	b_1	b_2	C_1	C_2
CG	-1/2	0.34	0.60	2.9	0.0087	0.10
SG	1/4	0.90	2.9	8.9	0.19	0.38

0.90, as indicated by arrow. Table I compiles the characteristic parameters for both CG and SG systems. It should be noted that the exponent β_2 for the CG system has the same value as that of β_1 for the SG one in the restricted range of ϕ, $0.34 < \phi < 0.90$.

In the following, we shall discuss the physical meaning of the characteristic value of ϕ_c (= 0.34 for CG and 0.90 for SG) obtained above using the concepts of a simple Ising spin model and a site-percolation picture.[21] For simplicity, we first consider a magnetic system consisting of N Ising spins. At the initial zero-field cooled state ($H = 0$, $T < T_g$), a magnetization M is zero, because the numbers of the up- and down-spins are equal (= $N/2$). When an external field is applied up to a peak field H_p, the number of the up-spins is increased by an amount of n, while that of the down-spins is decreased by n, and thus the magnetization at H_p is proportional to $2n$ [$M(H_p) \propto 2n$]. After the external field is switched off at $t = t_z$, the spin system will relax with time t (Fig. 7). At $t = t_z$, a partial amount of up-spins is decreased by an amount of n_1; the corresponding number of the down-spins is increased by n_1. Then the remanent magnetization $M_r(t_z)$ at $t = t_z$ is proportional to $2(n - n_1)$ [$M_r(t_z) \propto 2(n - n_1)$]. By definition, therefore, we have

$$\phi = 1 - M_r(t_z)/M(H_p) = n_1/n. \qquad (6)$$

On the other hand, such a spin system can be described by a site-percolation picture, as follows. The spin state at H_p corresponds to a lattice with $2n$ sites, while the magnetic state at $t = t_z$ corresponds to the situation, in which the n_1 sites of the lattice are occupied. Therefore, the volume fraction vp is written by $vp = n_1/2n = \phi/2$, where v is a filling factor of the lattice and p the fraction of the filled sites. In our case, the experimental values of $\phi_c/2$ for CG and SG systems are evaluated to be 0.17 and 0.45, respectively, which are in good agreement with the well-known values of the "critical volume fractions" 0.16 ± 0.02 for a three-dimensional (3D) lattice and 0.45 for a two-dimensional (2D) one.[21] In other words, we may say that the "percolation path" produced by the occupied n_1 sites (or the inversion of the n_1 spins up to $t = t_z$) is of 3D nature in the regime $0.34 < \phi < 0.90$ and of 2D one in $0.90 < \phi < 1$. Therefore, the fact that the exponent β_i for both CG and SG systems (Table I) has the same value in the regime $0.34 < \phi < 0.90$ suggests that β_i is a meaningful parameter to characterize the dimensionality of the percolation path.

3.2.1 Relaxation of Thermoremanent Magnetization (TRM)

Figure 10 shows the typical time variations for SG at 16.8 K of (a) the cooling-field H_{FC} = 0.14 T and (b) Hall resistivity, $\rho_H - R_0H$, where the time is set zero when the cooling-field begins to decrease; the normal Hall coefficient has been determined to be $R_0 = -7.4 \times 10^{-9}$ m^3/C, which is independent of temperature. The applied magnetic field H is decreased from the cooling-field H_{FC} (= 0.14 T) at a constant rate δH (= 10 T/s) and vanishes at time t_z (= $H_{FC}/\delta H$ = 14 ms), as indicated by arrows. We should note that t_z is very short compared with a waiting time t_w (= 180-18,000 s) and the time span of relaxation measurements (0-10^4 s). As the magnetic field is decreased to zero, the Hall resistivity decays with time from $\rho_H^{FC} - R_0H_{FC} = 1.4 \times 10^{-8}$ at $t = 0$ to $\rho_H(t_z) = 1.15 \times 10^{-8}$ Ωm at time t_z, and in zero field it continues to relax slowly. [Solid curve in Fig. 10(b) is calculated using Eqs. (24) and (25), which are obtained from the concept of domain theory, with the best-fit parameters (see later)].

Similar measurements were carried out at various cooling-fields and temperatures. In Fig. 11(a) are plotted against H_{FC} the values of $\rho_H^{FC} - R_0H_{FC}$ and $\rho_H(t_z)$ at $T/T_g \cong 0.6$ [T = 24.6 K for SG (solid and open circles) and T = 32.4 K for CG (solid and open squares)]. As the cooling-field

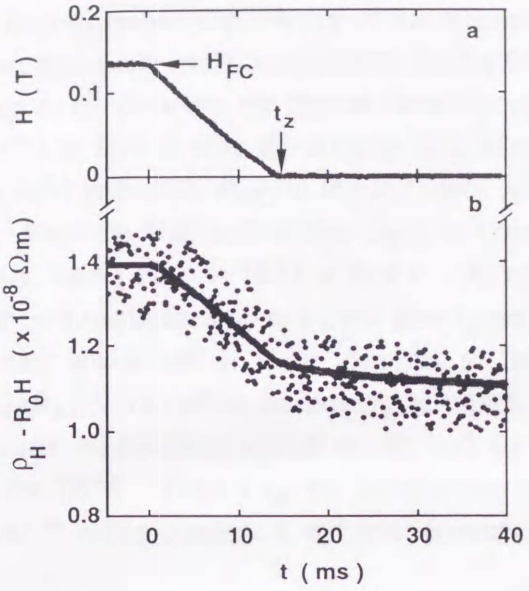

Fig. 10. Typical time variations at 16.8 K of (a) the external magnetic field from cooling-field H_{FC} (initially at 0.14 T) and (b) the Hall resistivity (ρ_H - R_0H) corresponding to the magnetization $M(t)$. Solid curve in Fig. 10(b) is calculated using Eqs. (24) and (25) with the best-fit parameters $m = 0.027$, $t_0 = 7 \times 10^{-6}$ s, $pz = 0.9$, $t_2^{pz}/t_1 = 0.0075$ s^{pz-1}, and $t_{\Delta H} = 40$ s (see text).

is increased, the value of ρ_H^{FC} - R_0H_{FC} is increased, indicating the enhancement of the magnetization,while the value of $\rho_H(t_z)$ tends to saturate at higher fields. The difference between

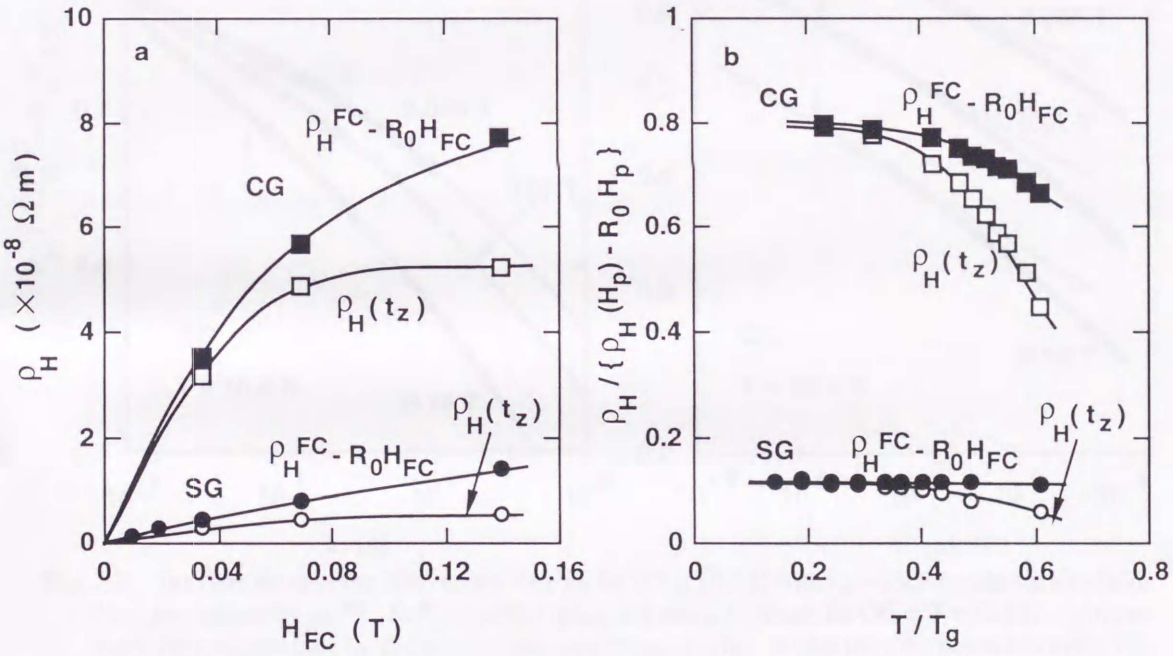

Fig. 11. (a) Magnetic field dependence of the Hall resistivities ρ_H^{FC} - R_0H_{FC} and $\rho_H(t_z)$ at $T/T_g \cong 0.6$ ($T = 26.8$ K for SG and those for CG = 32.4 K) and (b) temperature dependence of ρ_H^{FC} - R_0H_{FC} and $\rho_H(t_z)$ at a fixed magnetic fields $H_{FC} = 0.14$ T.

ρ_H^{FC} - R_0H_{FC} and $\rho_H(t_z)$ becomes appreciable with increasing H_{FC}; this difference is regarded as a quantity representing a 'relaxed' magnetization until the magnetic field vanishes (see later). On the other hand, in Fig. 11(b) we plot the temperature dependence of ρ_H^{FC} - R_0H_{FC} and $\rho_H(t_z)$, normalized by the saturated values $\rho_H(H_p)$ - R_0H_p using the data at 8.2 T (see Fig 8), at fixed magnetic field $H_{FC} = 0.14$ T. The ratio $[\rho_H^{FC} - R_0H_{FC}]/[\rho_H(H_p) - R_0H_p]$ shows a drastic decrease at higher temperature for CG, in contrast to almost temperature-independent behavior of SG that

reflects the temperature dependence of the magnetization (Fig. 1). In addition, we see that that ratio for SG are extremely small compared to that for CG.

Figure 12 illustrates the typical decay curves of Hall resistivities or TRM for (a) SG at 16.8 K and (b) CG at 32.4 K after the cooling-field is switched off with the waiting time t_w=1,800 s under different field intensities H_{FC} in log-log plots, where ρ_H is normalized by the initial value (ρ_H^{FC} - R_0H_p). Here the Hall resistivities $\rho_H(t)$ at time t is expressed by Eq. (2) with H = 0, as $\rho_H(t)$= $4\pi R_s M_r(t)$, where $M_r(t)$ is TRM at time t. As can be seen, in both SG and CG, all the experimental points lie on straight lines up to a lapse time t_d marked by arrows, beyond which the deviations become appreciable, which are in sharp contrast to the case of IRM. As done for a SG material of $Eu_{0.4}Sr_{0.6}S_4$,[22] we define the time t_d, at which the deviations from Eq. (3) begin to increase more than a quarter of the mean square errors, and we simply call it a 'deviation time' to specify the decay profiles for TRM. For $t < t_d$, the decay curve can be written by the power law of time as Eq. (3), $\rho_H(t) = At^{-m}$ with a constant A and an exponent m. Moreover, we have found no significant

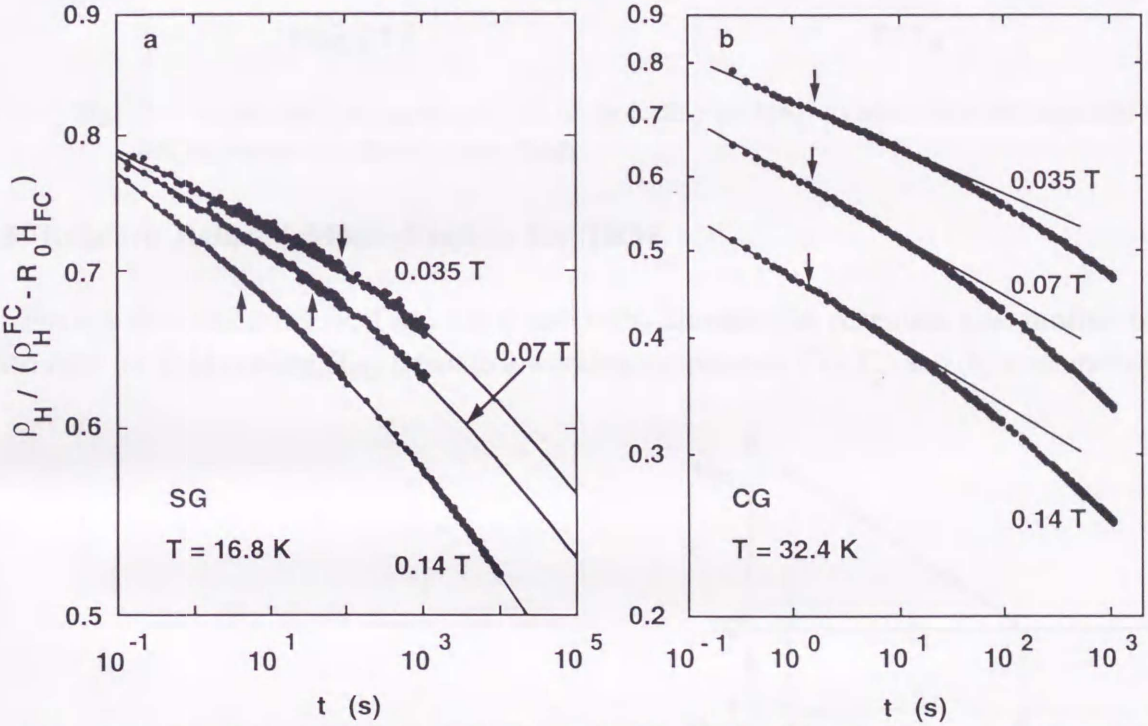

Fig. 12. (a) Time decay of the Hall resistivities ρ_H for SG at 16.8 K with t_w = 1800 s under various fields H_{FC}, normalized by (ρ_H^{FC} - R_0H_{FC}) at H_{FC} in log-log plots, (b) those for CG at T = 32.4 K. Arrows mark the deviation time t_d, above which the experimental points deviate from the power law of Eq. (3). Solid curves in Fig. 12(a) are calculated using Eq. (25) with the magnetic field-independent parameters pz = 0.9, t_2^{pz}/t_1 = 0.0075 s^{pz-1}, and field-dependent ones m, t_d, and $t_{\Delta H}$ (see text).

difference in the decay curves observed at different waiting times t_w (180 - 18,000 s) in the experimental conditions of H_{FC} (= 0.01-0.14 T) and temperatures T (= 7.8 - 29.3 K) for SG; we have not measured the waiting-time dependence of TRM for CG. [We shall discuss later these results in terms of an "overlap length" introduced by Bray and Moore.[23]] The exponent m for TRM is plotted against (a) the cooling-field at T/T_g = 0.6 and (b) against temperature at H_{FC} = 0.14 T in Fig. 13. It is apparent that the exponent m for SG increases linearly with increasing the cooling-field and it also increases drastically as the temperature is raised toward T_g; the behaviors for CG are almost the same as those for SG.

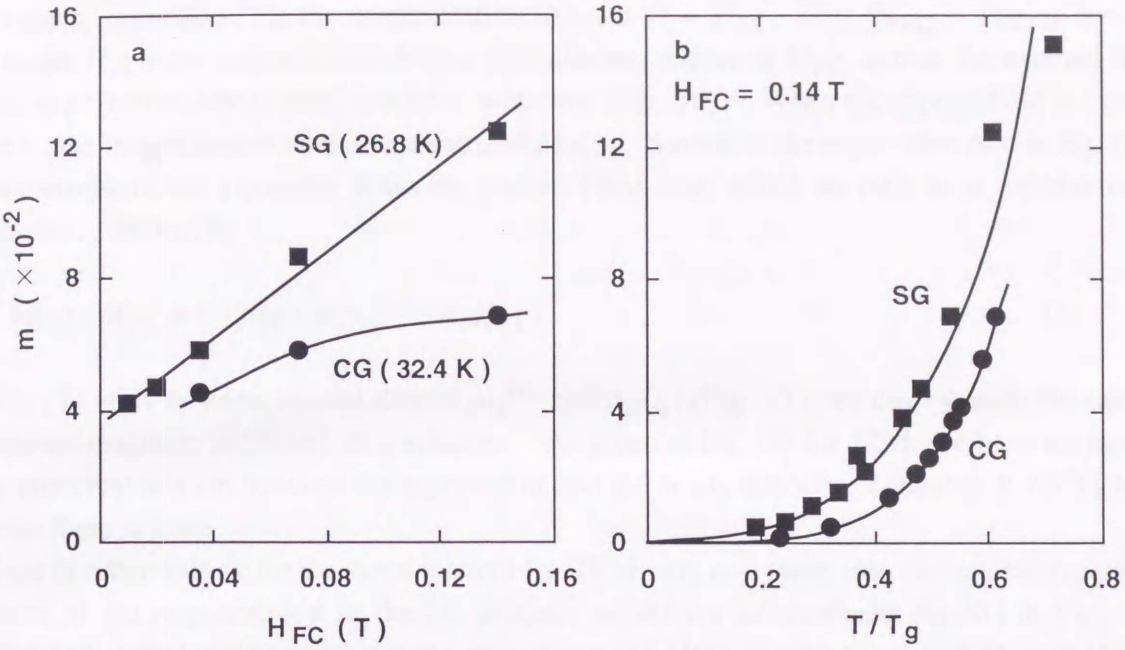

Fig. 13. Variations of the exponent m with (a) the cooling-field H_{FC} at various temperatures and (b) with temperature at different cooling-fields.

3.2.2 Relative Relaxed Magnetization for TRM

For our discussion below, Figs. 14(a) and 14(b) illustrate the schematic time profiles of (a) an applied field for field-cooling H_{FC} down to a working temperature T ($<T_g$) and (b) a magnetization

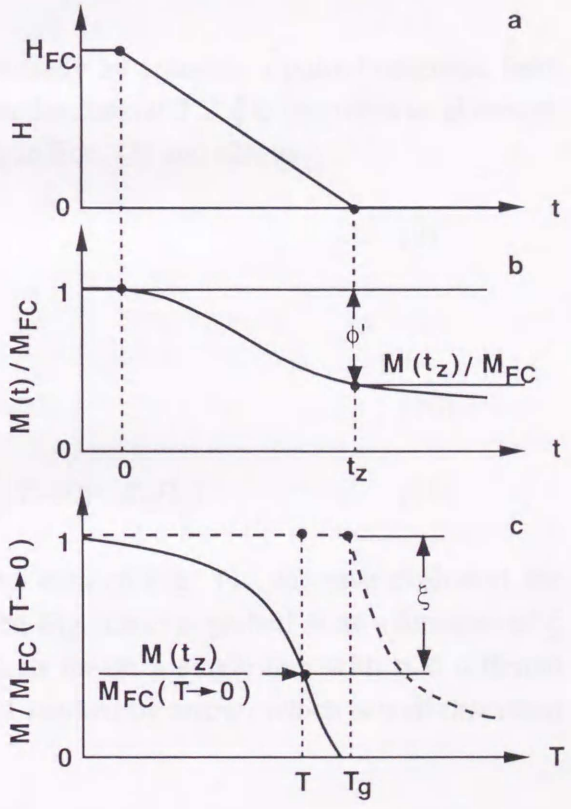

Fig. 14. Schematic time profile of (a) a field-cooling magnetic field H_{FC} and (b) a magnetization $M(t)$ at time t and temperature T ($< T_g$), normalized by the magnetization M_{FC} at H_{FC}, $M(t)/M_{FC}$, where the origin of the time is set when the applied field is switched off to zero; ϕ' is defined by Eq. (7). (c) Schematic temperature dependence of the magnetizations $M(t_z)$ at time $t = t_z$ and M_{FC} at $H = H_{FC}$, normalized by the value M_{FC} at absolute zero [here denoted by $M_{FC}(T\rightarrow 0)$]; solid line indicates $M_{FC}/M_{FC}(T\rightarrow 0)$ and broken one $M(t_z)/M_{FC}(T\rightarrow 0)$. ξ is a newly introduced quantity to characterize the dynamical properties for TRM, defined by Eq. (8).

$M(t)$ at time t, normalized by the magnetization M_{FC} at $H = H_{FC}$, $M(t)/M_{FC}$. During the field-cooling under H_{FC}, the magnetization $M(t)$ is held almost constant at M_{FC}, and as the external field is decreased at a constant rate to zero, it relaxes with time (Fig. 10). When the applied field is switched off at $t = t_z$, the magnetization attains to a value of $M(t_z)$. Similar to the expression of ϕ in Eq. (5) for IRM, we here introduce a quantity ϕ' for the present TRM case, which we refer to as 'relative relaxed magnetization', defined by

$$\phi' = 1 - M(t_z) / M_{FC} = 1 - \rho_H(t_z)/(\rho_H^{FC} - R_0 H_{FC}). \quad (7)$$

Using Eq. (7) with the experimental data of ρ_H^{FC} and $\rho_H(t_z)$ (Fig. 11), we can evaluate the values of ϕ' at different magnetic fields and temperatures. As given in Eq. (5) for IRM, we have attempted to find any universal relation between the exponent m and the newly introduced quantity ϕ' for TRM; but in this case there is none.

Then in order to look for a general relation for TRM, we have taken into account the temperature dependence of the magnetization in the FC process, as shown schematically for SG in Fig. 14(c). Here solid and dotted curves represent the magnetizations $M(t_z)$ at time $t = t_z$ and M_{FC} at $H = H_{FC}$ [Figs. 14(a) and 14(b)], normalized by the value M_{FC} at absolute zero [here denoted by $M_{FC}(T \to 0)$], respectively. The field-cooling under H_{FC} proceeds along the dotted curve from a high temperature, say $1.5T_g$, down to a working temperature T, where as the external magnetic field is decreased to zero, TRM is decreased along the dotted vertical line to the value $M(t_z)$ at $t = t_z$ (and further toward zero at infinite time). Using this picture, we now introduce a new dynamical quantity ξ as a 'relative relaxed magnetization' for TRM, as marked by arrow in Fig. 14(c), defined by

$$\xi = 1 - M(t_z) / M_{FC}(T \to 0). \quad (8)$$

Since a saturation magnetization $M^{sat}(T)$ obtained experimentally by applying a pulsed magnetic field with the peak field H_p=8.2 T is almost temperature independent below T_g, ξ is rewritten to eliminate the temperature-dependent extraordinary Hall coefficient R_s in Eqs. (1) and (2), as

$$\xi = 1 - [M(t_z) / M^{sat}(T)] / [M_{FC}(T \to 0)/M^{sat}(T \to 0)] \quad (9)$$

with

$$M(t_z) / M^{sat}(T) = \rho_H(t_z)/[\rho_H(H_p, T) - R_0 H_p], \quad (10)$$

$$M_{FC}(T \to 0)/M^{sat}(T \to 0) = [\rho_H^{FC}(T \to 0) - R_0 H_{FC}]/[\rho_H(H_p, T \to 0) - R_0 H_p]. \quad (11)$$

Using Eqs. (9)-(11), together with the experimental data of Fig. 11, we have evaluated the values of ξ at different temperatures and cooling fields. In Fig. 15(a) is plotted m as a function of ξ for SG in logarithmic scales, where the experimental points lie on a single line with two different slopes above and below the characteristic point of $\xi_c = 0.21$ marked by arrow, which is well described by the following expression,

$$m = D\xi^{\gamma}, \tag{12}$$

where the best-fit parameters are determined to be D =0.30 and γ = 1.4 for $\xi > \xi_c$ and D = 2.6 and γ = 2.8 for $\xi < \xi_c$. On the other hand, for CG, as shown in Fig. 15(b) in linear scales, we see that all the experimental points lie on a single line with the best-fit parameter D =0.15 and γ = 1.0. Thus Eq. (12) is regarded as a general expression to characterize the dynamics of TRM in the short time range less than t_d for both SG and CG of our magnetic material and ξ is a good parameter to describe the freezing state of SG and CG phases. We note that the γ value for SG (γ = 1.4 and 2.8) is larger than that for CG (γ = 1.0), which indicates that the dependence of m on ξ is much stronger in the former case than in the latter.

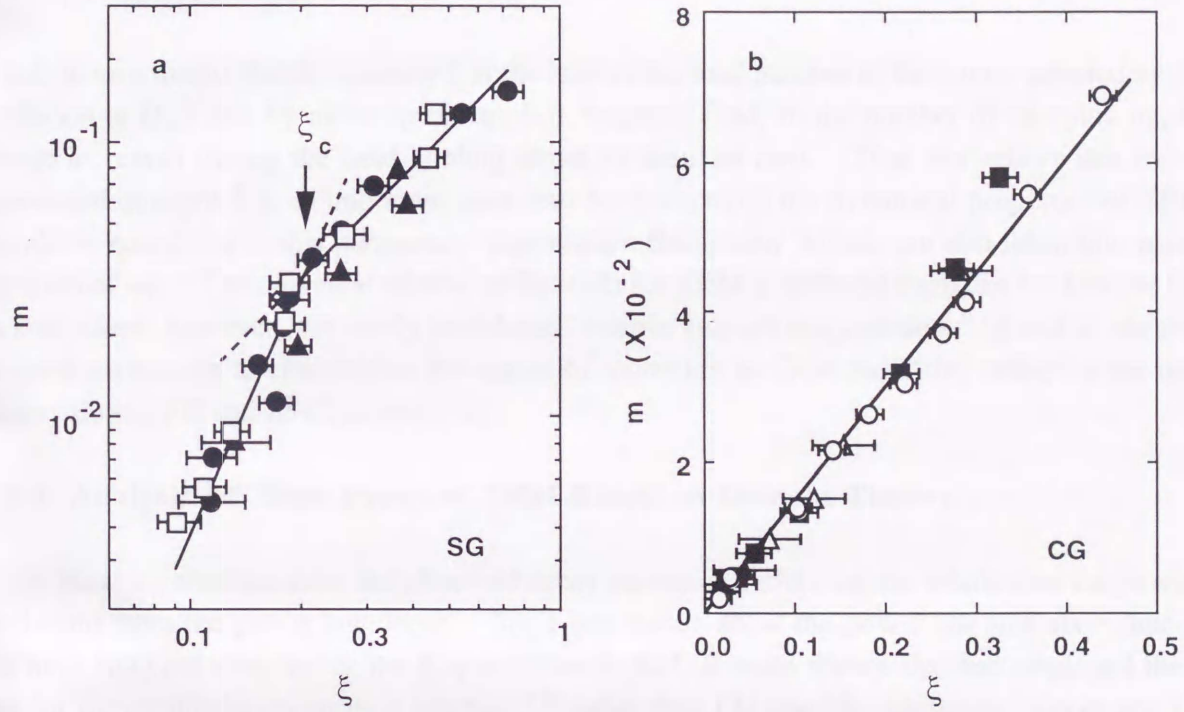

Fig. 15. (a) The exponents m plotted against ξ which can be expressed in the form of Eq. (12) (see text), (a) for SG arrow marks the characteristic values of ξ_C = 0.21 and (b) for CG phase.

Here we discuss the quantity ξ using the concept of a single Ising spin model for TRM, where for simplicity we consider a magnetic system consisting of N Ising spins, as done for IRM. At the initial state above T_g, a magnetization M is zero before applying H_{FC}; the number of the up- and down-spins are equal (=N/2). When a cooling-field H_{FC} is applied and the system is cooled down to a temperature T below T_g, the number of the up-spins is increased by an amount of $n_{FC}(T)$, while that of the down-spins is decreased by $n_{FC}(T)$, and thus the magnetization M_{FC} is proportional to $2n_{FC}(T)$. After the external field is switched off at $t = t_z$, the spin system will relax with time t. At $t = t_z$, a partial amount of up-spins is decreased by an amount of n_H; thus TRM or $M(t_z)$ at $t = t_z$ is proportional to $2[n_{FC}(T) - n_H]$. By definition, we have

$$\xi = 1 - M(t_z) / M_{FC}(T \rightarrow 0)$$

$$= \{ [M_{FC}(T \rightarrow 0) - M_{FC}] + [M_{FC} - M(t_z)] \} / M_{FC}(T \rightarrow 0). \tag{13}$$

We denote here the number of the increased up-spins $n_{FC}(T)$ at absolute zero by $n_{FC}(T\rightarrow 0)$ corresponding to the magnetization $M_{FC}(T\rightarrow 0)$. The first term in Eq. (13), $[M_{FC}(T\rightarrow 0) - M_{FC}]$, is proportional to $2[n_{FC}(T\rightarrow 0) - n_{FC}(T)]$, which we simply write as $2n_T$, where n_T is regarded as the number of thermally inverted spins out of the increased up-spins $n_{FC}(T\rightarrow 0)$. Here we may expect that the value of $2n_T$ of SG is much smaller than that of CG, from the temperature dependent magnetization curves (Fig. 1). In addition, the second term $[M_{FC} - M(t_z)]$, the difference in the magnetizations at temperature T before and after the external field is switched off [Fig. 14(c)], is proportional to $2n_H$. Then Eq. (13) is rewritten as,

$$\xi = (n_T + n_H)/n_{FC}(T\rightarrow 0), \tag{14}$$

which in turn means that the quantity ξ is the ratio of the total number of the spins, inverted by thermal excitation at H_{FC} and by reducing the applied magnetic field, to the number of up-spins $n_{FC}(T\rightarrow 0)$ that is increased during the field cooling down to absolute zero. Thus we believe that our newly introduced quantity ξ is an important parameter to characterize the dynamical properties of TRM. It should be noted that in this parameter, 'temperature fluctuation' effects are also taken into account in the form of n_T. The universal relation of Eq. (12) for TRM is different from that for IRM of Eq. (5). In both cases, however, the newly introduced 'relative relaxed magnetization', ξ and ϕ, are regarded as good parameters to characterize the degree of relaxation in TRM and IRM, reflecting the magnetic history during FC and ZFC, respectively.

3.2.3 Analysis of Time Decay of TRM Based on Domain Theory

Now we shall consider the observed decay curves of TRM over the whole time range where the deviations from the power law occur. Since our results show the power law in a short time region, we have analyzed them using the Koper-Hilhorst (KH) domain theory that has employed the power law for the equilibrium relaxation function,[15] rather than FH one.[14] However, Koper and Hilhorst have derived theoretical expressions with an idealized stepwise form for switching off of an external cooling-field H_{FC}, whereas in our actual experiments it is decreased at a constant rate δH to zero within the time t_z. Thus we need some modifications of their expressions, as described below.

According to the KH model, the magnetization is expressed, by assuming that a linear response theory is valid for relaxation of SG, as

$$M(t) = \Delta M(t) + N\chi_{eq}H(t) = -N\chi_{eq}\int_0^t dt'\, R(t,t')\dot{H}(t') + N\chi_{eq}H(t), \tag{15}$$

where $\Delta M(t)$ is an excess magnetization, N the number of spins in a sample, and χ_{eq} the equilibrium dc susceptibility in zero field. Based on the experimental data[24] and Monte Carlo simulations,[25] the relaxation function $R(t, t')$ is written as,

$$R(t, t') = R_{eq}(t - t')F(t, t'). \tag{16}$$

In thermal equilibrium $R_{eq}(t - t')$ is given by,

$$R_{eq}(t - t') = [1 + (t - t')/t_0]^{-m}, \tag{17}$$

where t_0 specifies a minimum relaxation time in the equilibrium relaxation spectrum, as discussed in section **3.2.4**. A plausible choice for $F(t, t')$ is a cutoff reflecting deviations from equilibrium, $F(t, t') = \exp[-(t - t')/\tau_{max}(s)]$, where $\tau_{max}(s)$ is a maximum relaxation time in the relaxation spectrum of a size s domain, and a plausible generalization of $F(t, t')$ using the time dependent domain size $s(t'')$ ($t' < t'' < t$) gives

$$F(t, t'; [s(t'')]) = \exp\{-\int_{t'}^{t} dt''/\tau_{max}[s(t'')]\}. \tag{18}$$

Due to the spin coherence within a domain, $\tau_{max}(s)$ is assumed to be a function of domain size with a typical spin spacing a,

$$\tau_{max}(s) \cong t_1(s/a)^z, \tag{19}$$

where t_1 is a microscopic time constant and z a dynamical parameter.

Furthermore, Bray and Moore[23] have predicted that during the waiting time t_w the domain size $s(t)$ cannot grow larger than an "overlap length" $l_{\Delta H}$ for a given magnetic field jump ΔH (in our case H_{FC}), which is written as $l_{\Delta H} \sim |\Delta H|^{-2/(d - 2y)}$ with the dimension of the system d and a constant y. Taking account of the interplay between $s(t)$ and $l_{\Delta H}$, the KH model considers the following two cases: For a small field jump, $s(t_w) < l_{\Delta H}$, the domain size $s(t)$ increases as a power of time,

$$s(t) \cong a[(t_w + t)/t_2]^p, \tag{20}$$

where t_2 is a microscopic time and p another dynamical parameter. For a large field jump, where the linear size of domains reaches its upper limit $l_{\Delta H}$ during the waiting time t_w, $s(t_z) = l_{\Delta H}$, and thus $s(t)$ is written as, for $t > t_z$,

$$s(t) \cong a[(l_{\Delta H}/a)^{1/p} + (t - t_z)/t_2]^p. \tag{20'}$$

In this expression, the waiting time t_w does not enter, indicating that it does not affect the domain size after the switching-off of the external field. Since there is no t_w dependence of the observed decay curves, therefore, we use Eq. (20') for the time dependence of the domain size. In addition, a time $t_{\Delta H}$ is defined, during which the domain is growing up to a size of $l_{\Delta H}$, as

$$t_{\Delta H} = t_2[(l_{\Delta H}/a)]^{1/p} \sim |\Delta H|^{-2/[(d - 2y)p]}. \tag{21}$$

With this quantity and using Eqs. (19) and (20'), the maximum relaxation time is given by,

$$\tau_{max}(t) = (t_{\Delta H} + t - t_z)^{pz}(t_2^{pz}/t_1)^{-1}. \tag{22}$$

The time decays of TRM can be calculated using the above expressions. Taking account of the time dependent magnetic field change at a constant rate δH in our case, not stepwise as in the KH model, we express the time variation of the magnetic field, with $t_z = H_{FC}/\delta H$, as

$$H(t) = H_{FC} - t\delta H \quad \text{for } 0 \le t \le t_z,$$

$$= 0 \quad \text{for } t > t_z. \tag{23}$$

In the time region $t \le t_z$ we may take $F(t, t') = 1$ since $t - t' << \tau_{max}(s)$, and we get

$$M(t) = N\chi_{eq}\delta H\,[-t_0/(-m+1)][1 - (1 + t/t_0)^{-m+1}] + N\chi_{eq}(H_{FC} - t\delta H). \tag{24}$$

On the other hand, in the case for $t > t_z$, $F(t, t') \neq 1$, yielding

$$M(t) = \Delta M(t) = N\chi_{eq}\delta H \int_0^{t_z} dt'[1 + (t - t')/t_0]^{-m}$$

$$\times \exp\{[(t_{\Delta H} + t - t_z)^{1-pz} - (t_{\Delta H} + t' - t_z)^{1-pz}]t_2^{pz}/[t_1(1 - pz)]\}. \tag{25}$$

The above integration cannot be carried out analytically and therefore we have made the numerical integration to calculate TRM. For the numerical calculations of Eqs. (24) and (25), we have assumed the following conditions for fitting parameters: i) we take the observed exponent m, ii) pz is a universal constant independent of temperature and magnetic field, iii) the ratio t_2^{pz}/t_1 is a function of temperature alone, and iv) both t_0 and $t_{\Delta H}$ depend on temperature and magnetic field.

As an example for SG, solid line in Fig. 10(b) shows the calculated curve of the Hall resistivity (or TRM) using Eqs. (24) and (25) with the best-fit values of $m = 0.027$, $t_0 = 7 \times 10^{-6}$ s, $pz = 0.9$, $t_2^{pz}/t_1 = 0.0075$ s^{pz-1}, and $t_{\Delta H} = 40$ s in the time range $t = 0$-40 ms, where the cooling-field is decreasing at the constant rate 10 T/s, in satisfactory agreement with the observation. Furthermore, we have performed the numerical calculations of the overall time decays of TRM at various conditions (temperatures and cooling-field intensities) using Eq. (25) to obtain reasonable agreements with the experiments, as shown by solid curves in Fig. 12(a); the parameters used for the calculations are the field-independent ones ($pz = 0.9$, $t_2^{pz}/t_1 = 0.0075$ s^{pz-1}), and the field-dependent ones ($m = 0.018$, 0.022, 0.027, $t_0 = 9 \times 10^{-8}$, 7×10^{-7}, 7×10^{-6} s, $t_{\Delta H} = 350$, 130, 40 s for $H_{FC} = 0.035$, 0.07, 0.14 T, respectively). We shall discuss the obtained dynamical parameters below.

3.2.4 Equilibrium Relaxation — Power law

Now we shall pay attention to the dynamical parameters t_0 and exponent m of the equilibrium relaxation function $R_{eq}(t - t')$ in Eq. (17). For a system with a distribution function of relaxation time τ, $P(\tau)$, the equilibrium relaxation function is given by $R_{eq}(t - t') = \int d\tau P(\tau)\exp[(t - t')/\tau]$. Using an inverse Laplace transform, we can get $P(\tau)$ corresponding to $R_{eq}(t - t')$ with the power law form in Eq. (17),

$$P(\tau) = [t_0/\Gamma(m)](\tau/t_0)^{-(m+1)}\exp(-t_0/\tau), \tag{26}$$

where $\Gamma(m)$ is a Gamma function of m. In terms of the relaxation spectra $Q(\tau)$, which is defined by $R_{eq}(t - t') = \int d(\ln\tau) Q(\tau) \exp[(t - t')/\tau]$, we obtain

$$Q(\tau) = [1/\Gamma(m)](\tau/t_0)^{-m} \exp(-t_0/\tau). \qquad (26')$$

From the form of Eq. (26'), we see that t_0 is a minimum relaxation time and m characterizes the distribution intensity and width of the relaxation spectrum.

The best-fit parameters t_0 obtained at different magnetic fields are plotted against temperature in Fig. 16. With increasing temperature, the values of t_0 increase appreciably from 10^{-13}-10^{-12} s at around 8 K and tend to saturate above 18 K to the values as high as 10^{-6}-10^{-4} s. We also note that t_0 increases with the cooling-field H_{FC}. The magnitude of t_0 for our system is comparable with those for the insulating SG of $CdCr_{1.7}In_{0.3}S_4$ ($t_0 \sim 10^{-15}$ s)[15] and $Fe_{0.5}Mn_{0.5}TiO_3$ ($t_0 = 10^{-6}$-10^{-5} s estimated from the reported decay curves)[6].

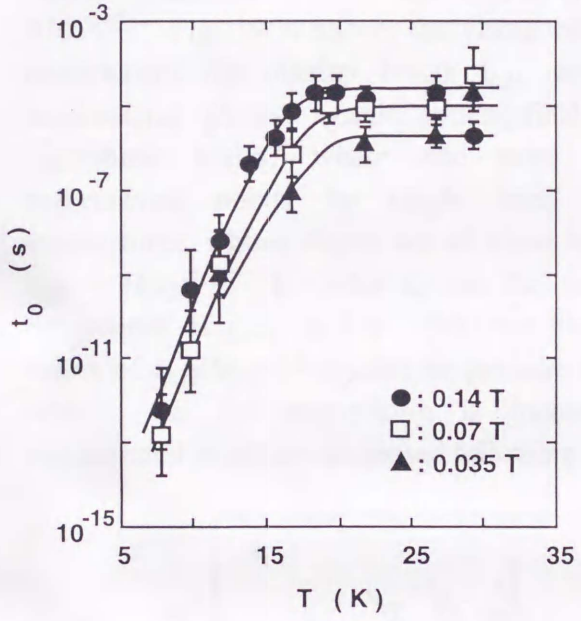

Fig. 16. The best-fit values of minimum relaxation time t_0 of SG at different cooling-fields H_{FC} plotted against temperature.

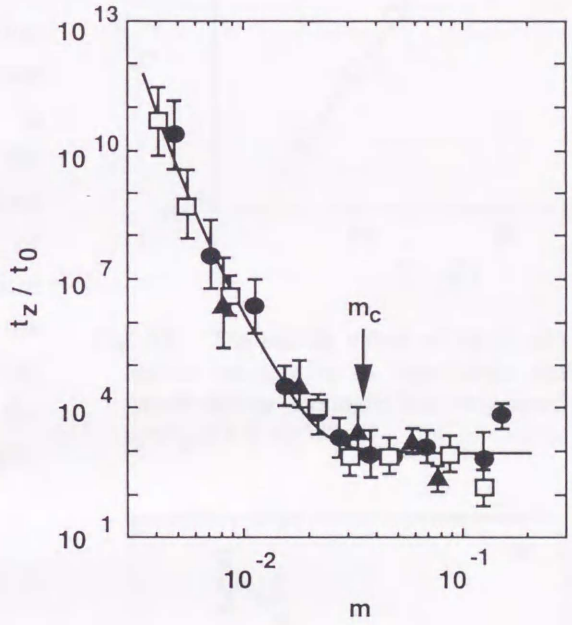

Fig. 17. The values of t_z/t_0 plotted against m; symbols are the same as those in Fig. 16, arrow marks $m_C = 0.033$.

Now using the dynamical parameters m and t_0, the RRM parameter ξ, as mentioned above, can be expressed as given below. The magnetizations in ξ are written as $M^{FC}(T\to0) = N\chi_{eq}(T\to0)H_{FC}$ and $M(t_z) = N\chi_{eq}(T)\delta H[-t_0/(-m + 1)][1 - (1 + t_z/t_0)^{-m+1}] \sim N\chi_{eq}(T)H_{FC}(t_z/t_0)^{-m}/(-m + 1)$, and thus ξ is rewritten as

$$\xi = 1 - M(t_z)/M^{FC}(T\to0) \sim 1 - [\chi_{eq}(T)/\chi_{eq}(T\to0)](t_z/t_0)^{-m}/(-m + 1). \qquad (27)$$

Since $\chi_{eq}(T)/\chi_{eq}(T\to0) \sim 1$ for general SG cases, including our results [see Fig. 11(b)], we get a simple form,

$$\xi \sim 1 - (t_z/t_0)^{-m}/(-m + 1). \qquad (27')$$

The values of t_z/t_0 are plotted against m in Fig. 17. With increasing m, t_z/t_0 decreases and becomes nearly constant above $m_C = 0.033$, marked by arrow, which corresponds to the characteristic value ξ_C (= 0.21) that represents the turning point where the minimum relaxation time t_0 (or t_z/t_0) depends on the temperature or not.

3.2.5 Nonequilibrium Relaxation

In a nonequilibrium relaxation, the maximum relaxation time $\tau_{max}(t)$ [= $(t_{\Delta H} + t - t_z)^{pz}(t_2^{pz}/t_1)^{-1}$] in Eq. (22) is an important quantity that characterizes the upper cutoff in the relaxation spectra of time-dependent domains. In Fig. 18 are plotted the best-fit values of t_2^{pz}/t_1 against temperature in logarithmic scales, which follow well a single line, as $t_2^{pz}/t_1 = 2.8 \times 10^{-5}T^2$. Fig. 19(a) shows the values of $t_{\Delta H}$, that characterizes the overlap length $l_{\Delta H}$, at different temperatures plotted against cooling-field H_{FC} in logarithmic scales, where one notes that the experimental points lie single lines at fixed temperatures, whose slopes are all equal to -1.5, or $t_{\Delta H} \sim H_{FC}^{-1.5}$. In order to see the temperature dependence of $t_{\Delta H}$, in Fig. 19(b) we illustrate the values of $t_{\Delta H}/H_{FC}^{-1.5}$ against temperature in log-log plots. As the temperature is increased, the experimental points are decreased following a straight

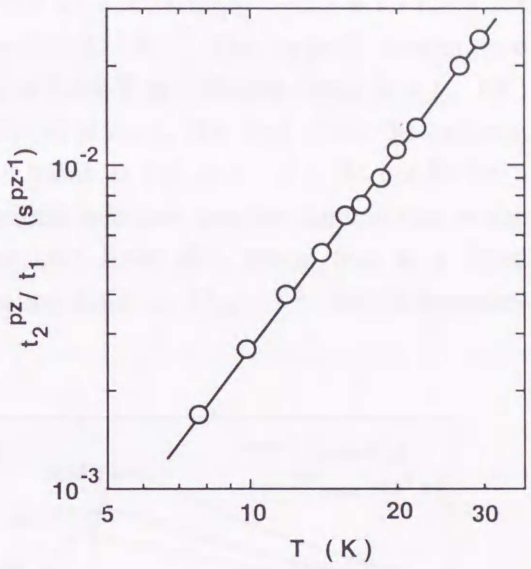

Fig. 18. The best-fit values of t_2^{pz}/t_1 plotted against temperature in logarithmic scales, which follow a single line, expressed as $t_2^{pz}/t_1 = 2.8 \times 10^{-5}T^2$.

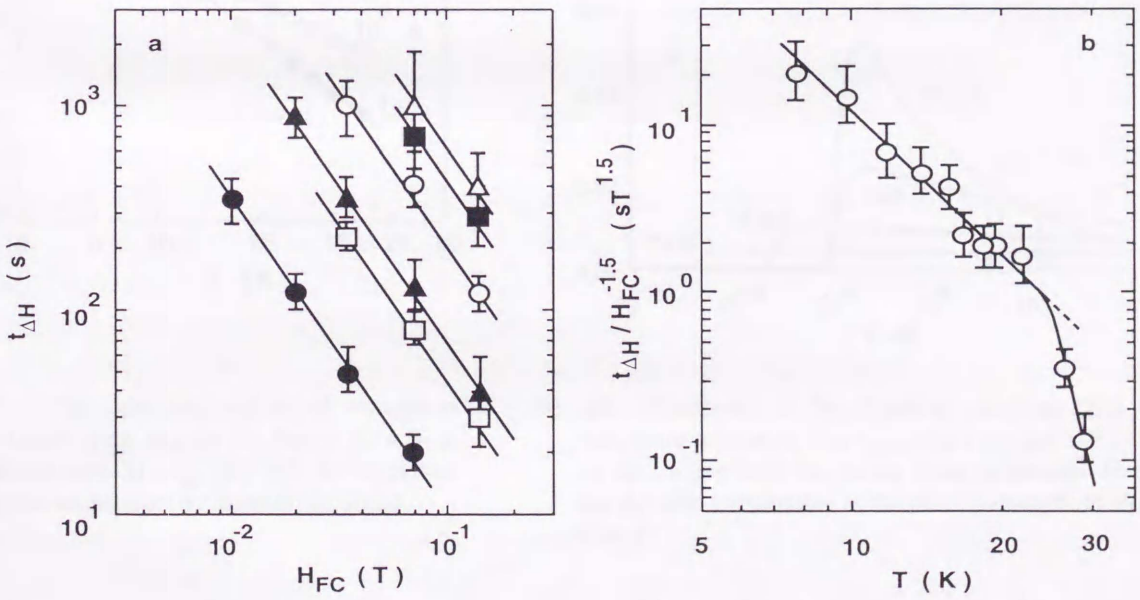

Fig. 19. (a) The best-fit values of $t_{\Delta H}$ at different temperatures plotted against the cooling-field H_{FC} in logarithmic scales; symbols from open triangles to solid circles correspond to the temperatures 7.8, 9.8, 11.8, 16.8, 21.8 and 26.8 K, respectively. The slope of each line is all equal to -1.5, which corresponds to $-2/[(d - 2y)p]$ in Eq. (21). (b) The values of $t_{\Delta H}/H_{FC}^{-1.5}$ plotted against temperature.

line up to a temperature of about 20-25 K ($\cong T_g/2$), as $t_{\Delta H}/H_{FC}^{-1.5} = 1.2 \times 10^4 T^{-3}$, above which they show a steep decrease; such drastic temperature variations are also found in other quantities, such as $\rho_H(t_z)$ [Fig. 11(b)] and m [Fig. 13(b)]. We should note that the ratio t_2^{pz}/t_1 exhibits no drastic variation around that temperature (Fig. 18), while the value of $t_{\Delta H}$ or t_2 [see Eq. (21)] changes appreciably, which means that the time constant t_1 is also reduced markedly above 20-25 K. These results indicate that thermal fluctuations in spin-glass system becomes appreciable above this temperature.

From Figs. 18 and 19, we obtain $\tau_{max}(t)=3.6 \times 10^4 T^{-2} \times (1.2 \times 10^4 H_{FC}^{-1.5} T^{-3} + t - t_z)^{0.9}$ for the maximum relaxation time at low temperatures below 20-25 K. The typical temperature dependence of the maximum relaxation time $\tau_{max}(t)$ for $H_{FC} = 0.14$ T at different times ($t = t_z$, 10^2, 10^3, 10^4 s) are shown in Fig. 20 in logarithmic scales; the curves at $t = t_z$ (the time when the external field is reduced to zero) and 10^4 s follow a straight line, but those at 10^2 and 10^3 s do not lie on a straight line. We see that $\tau_{max}(t)$ is increased with time t, which indicates that the domain size in the SG system grows as time laps. Though not shown here, we have also found that at a fixed temperature $\tau_{max}(t)$ at $t = t_z$ depends strongly on the cooling-field as $H_{FC}^{-1.35}$, but it becomes independent of H_{FC} for $t >> t_z$.

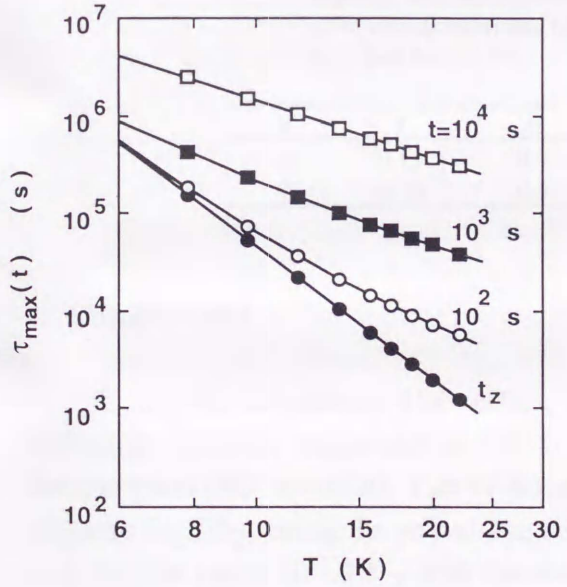

Fig. 20. The calculated values of maximum relaxation time $\tau_{max}(t)$ for $H_{FC} = 0.14$ T at different times ($t = t_z$, 10^2, 10^3, 10^4 s) plotted against temperature in logarithmic scales.

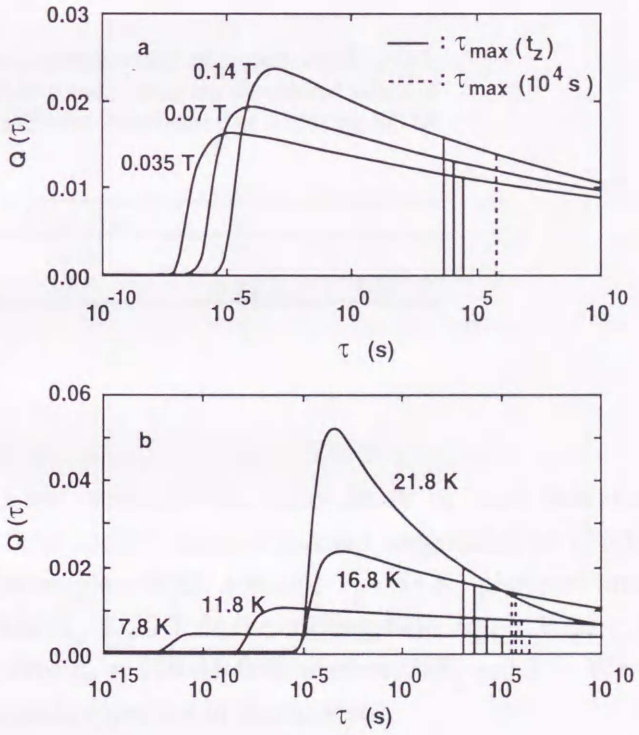

Fig. 21. Variations of the relaxation spectrum $Q(\tau)$ and maximum relaxation time $\tau_{max}(t)$ at $t = t_z$ and 10^4 s with (a) the cooling-field H_{FC} at the fixed temperature 16.8 K and (b) with temperature at the fixed cooling-field $H_{FC} = 0.14$ T.

Moreover, Fig. 21 illustrates the relaxation spectra $Q(t)$ for TRM calculated using Eq. (26') with the parameters t_0 and m obtained, together with the maximum relaxation time $\tau_{max}(t)$ at $t = t_z$ (solid lines) and 10^4 s (broken lines). As shown in Fig. 21(a), with increasing the cooling-field H_{FC}, the lower cutoff t_0 shifts to a longer time side with the increased intensity and slope, while the higher

cutoff $\tau_{max}(t)$ at $t = t_z$ becomes shorter but at $t = 10^4$ s it is independent of H_{FC}. The relaxation spectrum depends remarkably on temperature, as shown in Fig. 21(b) for a typical case of $H_{FC} = 0.14$ T. The lower cutoff shifts to a longer time side with raising temperature up to 16.8 K, above which it becomes almost constant, and the relaxation spectrum is narrowed; the upper cutoff also shifts gradually to a shorter time side. These results are in qualitative agreement with those obtained from Monte Carlo simulations in the temperature range $0.6 < T/T_g < 2$ for two-dimensional Ising SG by Nemoto and Takayama,[26] where they have assumed that the longer relaxation time represents the dynamical aspect associated with overturn of the spin cluster to which the spin belongs, while the shorter relaxation time represents the fast relaxation associated with the local excitation of each spin.

Finally, we have evaluated the dynamical parameters for TRM of our SG system. From $t_{\Delta H} \sim H_{FC}^{-1.5}$, we have $-2/[(d - 2y)p] = -1.5$ in Eq. (21). With this value, the parameters p and z are evaluated using the theoretical value of y for two-dimensional ($d = 2$) and three-dimensional ($d = 3$) Ising model by Bray and Moore.[23] Together with the theoretical values, our estimated values are listed in Table II ($p \sim 0.5$, $z \sim 2$), which are in good agreement with those estimated by Koper and Hilhorst[15] using the experimental data for insulating SG of $CdCr_{1.7}In_{0.3}S_4$ by Alba *et al.*[24] It is of interest to note that these dynamical parameters p and z are independent of insulating Ising SG or our itinerant magnetic SG.

Table II. Best-fit parameters obtained experimentally of pz and $-2/[(d - 2y)p]$, together with the evaluated values p and z using the theoretical values of y for two-dimensional ($d = 2$) and three-dimensional ($d = 3$) Ising SG by Bray and Moore.[23]

d	y	pz	$-2/[(d-2y)p]$	p	z
3	0.19	0.9	-1.5	0.51	1.8
2	-0.29	0.9	-1.5	0.52	1.9

4. Conclusions

Using the anomalous Hall effect, we have measured the time decay of zero-field cooled isothermal remanent magnetization (IRM) and field-cooled thermoremanent magnetization (TRM) in the spin-glass (SG: $x = 0.20$, $T_g = 41$ K) and cluster-glass (CG: $x = 1/4$, $T_g = 53$ K) phase of itinerant magnetic Fe_xTiS_2, using the pulsed magnetic field $H_p \leq 20$ T or the cooling-field $H_{FC} = 0.01$-0.14 T over the time range 10^{-2}-10^4 s with the waiting time $t_w = 180$-$18{,}000$ s below $T/T_g \sim 0.7$. We have found the following salient features of the dynamical properties in this material:

(A) In the case of IRM, the temperature and peak field dependencies of $\rho_H(t)$ are analyzed to obtain a universal relationship, $mT^{\alpha} = C\phi^{\beta}$, for the parameters characterizing the dynamical properties, where m is an exponent for the power law $\rho_H(t) = At^{-m}$ after a field is switched off, ϕ a newly introduced quantity, $\phi = [M(H_p) - M_r(t_z)] / M(H_p)$ [$M(H_p)$ is the magnetization at the peak field H_p and $M_r(t_z)$ the remanent magnetization at time $t = t_z$]. The exponent $\alpha = 1/4$ and $-1/2$ for SG and CG, respectively. The exponent β for SG and CG phases, has different values for $\phi < \phi_c$ and $\phi > \phi_c$ and $\phi_c = 0.90$ and 0.34, respectively, which corresponds to a two- and three-dimensional "critical volume fraction" in a site-percolation picture.

(B) In the short time regime $t < t_d$, the time decay of the Hall resistivity for TRM after the switching off of the external field can be expressed in the form of power law $\rho_H(t) = At^{-m}$, whose the

exponent m depends on both cooling-field H_{FC} and temperature T, while for $t > t_d$ deviations from the power law become appreciable. As found for both SG and CG phases, the magnetic field and temperature dependent exponent m is written in the universal form, $m = D\xi^{\gamma}$, where ξ [$= 1 - M(t_z)/M^{FC}(T \rightarrow 0)$] is a parameter of "relative relaxed magnetization" (RRM) for TRM, with the best-fit values for SG of $D = 0.30$, $\gamma = 1.4$ for $\xi > \xi_C$ ($= 0.21$) and $D = 2.6$, $\gamma = 2.8$ for $\xi < \xi_C$, the γ values being larger than that for CG ($D = 0.15$, $\gamma = 1.0$). Moreover, using the dynamical parameters appearing in the domain theory, we can express the parameter of relative relaxed magnetization ξ that characterizes the temperature and cooling-field dependence of the time decays of TRM for SG phase in a short time span, in the form $\xi \sim 1 - (t_z/t_0)^{-m}/(-m + 1)$, which is a function of t_z/t_0 and the exponent m.

(C) Using the "domain theory" developed by Koper and Hilhorst, numerical calculations for the observed decay curves of TRM of SG phase, over the whole time range have been performed with modifications of their theoretical expressions. As a result, we have found a satisfactory agreement between the simulations and experiments, including the independence of the TRM decays on the waiting time. The minimum relaxation time t_0 in the relaxation spectrum is increased with increasing temperature up to 18 K, above which it becomes constant (of the order of 10^{-5}-10^{-7} s), while the upper limit $\tau_{max}(t)$ depends on time, temperature, and cooling-field H_{FC}, which is expressed empirically as $\tau_{max}(t) = 3.6 \times 10^4 T^{-2} \times (1.2 \times 10^4 H_{FC}^{-1.5} T^{-3} + t - t_z)^{0.9}$ that has been obtained from the observed parameters t_2^{pz}/t_1 and $t_{\Delta H}$ with the best-fit value of $pz = 0.9$. Using these parameters, the equilibrium relaxation spectra are calculated; the spectra become narrowed with increasing temperature and cooing-field, which are in qualitative agreement with the Monte Carlo simulations for two-dimensional Ising SG.[26]

(D) With the evaluated value $2/[(d - 2y)p] = 1.5$ and the theoretical value of y for two-dimensional ($d = 2$) and three-dimensional ($d = 3$) Ising model, we have obtained the dynamical parameters $p \sim 0.5$ (a domain size increases as a power of time with the exponent of p) and $z \sim 2$ (the upper relaxation time depends on the domain size with the exponent of z), in agreement with those of some insulating Ising SG. With regard to the nature of magnetism (localized spin or itinerant electron picture), there are no differences in these dynamical parameters. More studies of relaxation phenomena, such as temperature cycle, will be desirable from another viewpoint of the hierarchical kinetics for our itinerant magnetic material.

Acknowledgments

The author would like to express his sincere thanks to Professor M. Inoue for valuable advice and continuing encouragement in the course of the present work. He is also grateful to Professor H. Takayama (Institute of Solid State Physics) and V.A.Kulbachinskii (Moscow State University) for valuable discussions. The author also thanks Associate Professor M. Sasaki and Drs. H. Negishi, M. Koyano, S. Ôhara, G.X. Tai, W.X. Gao,and K. Takase for fruitful discussions. Part of this work was supported by the Grants from Asahi Glass, Ogasawara Science Foundations, and Grant-in-Aid from the Ministry of Education, Science and Culture of Japan. Furthermore, he is indebted to colleagues and students in Inoue Laboratory for useful discussions and their help in taking the experimental data. At last, he thanks Ms. Y. Tahara and M. Sakata and J. Koyama and Mrs. Y. Nishigaki for their encouragements.

References

1) M. Inoue, H. P. Hughes and A. D. Yoffe: Adv. Phys. **38** (1989) 565.
2) H. Negishi, A. Shoube, H. Takahashi, Y. Ueda, M. Sasaki and M. Inoue: J. Magn. Magn Mater. **67** (1987) 179.
3) H. Negishi, H. Takahashi and M. Inoue: J. Magn. Magn. Mater. **68** (1987) 271.
4) H. Negishi, M. Koyano, M. Inoue, T. Sakakibara and T. Goto: J. Magn. Magn. Mater. **74** (1988) 27.
5) M. Koyano, M. Suezawa, H. Watanabe and M. Inoue, J. Phys. Soc. Jpn. **63** (1994) 1114.
6) A. Ito, H. Aruga, E. Torikai, M. Kikuchi, Y. Syono and H. Takei, Phys. Rev. Lett. **57** (1986) 483.
7) D. Sherrington and S. Kirkpatrick: Phys. Rev. B**17** (1978) 4384.
8) G. Parisi: Phys. Rev. Lett. A**73** (1979) 203.
9) G. Parisi: Phys. Rev. Lett. **50** (1983) 1946.
10) J. Hammann, M. Lederman, M. Ocio, R. Orbach, and E. Vincent: Physica A **185** (1992) 278.
11) F. Lefloch, J. Hammann, M. Ocio, and E. Vincent: Europhys. Lett. **18** (1992) 647.
12) M. Lederman, R. Orbach, J.M. Hammann, M. Ocio, and E. Vincent: Phys. Rev. B**44** (1991) 7403.
13) C. M. Newman and D. L. Stein: Phys. Rev. B**46** (1992) 973.
14) D.S. Fisher and D.A. Huse: Phys. Rev. Lett. **56** (1986) 1601.
15) G.J.M. Koper and H.J. Hilhorst: J. Physique. **49** (1988) 429.
16) P. Granberg, L. Lundgren, and P. Nordblad: J. Magn. Magn. Mater. **92** (1990) 228.
17) M.Inoue and H.Negishi: J. Phys Soc. Jpn. **53** (1984) 943.
18) C. M. Hurd: *The Hall Effect in Metals and Alloys* (Plenum Press, New York, 1972) chap. 5.
19) E. I. Kondrskii: Soviet Phys. JETP, **28** (1969) 291.
20) J. Ferré and N. Bontemps: Materials Science Forum **50** (1989) 21.
21) R. Zallen: *The Physics of Amorphous Solids* (John Wiley & Sons, New York, 1983) chap. 4.
22) N. Bontemps and R. Orbach: Phys. Rev. B**37** (1988) 4708.
23) A.J. Bray and M.A. Moore: Phys. Rev. Lett. **58** (1987) 57.
24) M. Alba, E. Vincent, J. Hammann, and M. Ocio: J. Appl. Phys. **61** (1987) 4092.
25) A.T. Ogielski: Phys.Rev B**32** (1985) 7384.
26) K. Nemoto and H. Takayama: J. Phys. C **16** (1983) 6835.

公表論文

① Y. Hara, W. X. Gao, H. Negishi, and M. Inoue:
Relaxation Behaviors in Cluster-Glass Phase of Itinerant Magnetic Fe_xTiS_2 Crystals Studied by Magnetotransport Measurements under Pulsed Magnetic Fields,
J. Magn. Magn. Mat.**135** (1994) 311.

② Y. Hara, H. Negishi, M. Sasaki, M. Inoue, and V. A. Kulbachinskii:
Time Decay of Thermoremanent Magnetization in Cluster-Glass Phase of Intercalation Compound Fe_xTiS_2 Studied by Use of Anomalous Hall Effect,
J. Magn. Magn. Mat. **145** (1995) 157.

③ Y. Hara, H. Negishi, M. Sasaki, and M. Inoue:
Relaxation of Thermoremanent Magnetization in Spin-Glass Phase of Itinerant Magnetic Fe_xTiS_2,
J. Magn. Magn. Mat. (1996) (in press).

参考論文

1) M. Koyano, S. Ôhara, Y. Hara, M. Inoue, G. Kido, and Y. Nakagawa:
High Magnetic Field Transport Properties of η-Mo_4O_{11} Crystals,
J. Phys. Soc. Jpn. **62** (1993) 1676.

2) V. A. Kulbachinskii, P. D. Maryanchuk, I. A. Churilov, M. Inoue, M. Sasaki, H.Negishi, and Y. Hara:
Electronic and magnetic properties of diluted magnetic semiconductor
$Hg_{1-x}Mn_xTe_{1-y}Se_y$,
Semicond. Sci. and Technol. **10** (1995) 463.

3) H. Negishi, Y. Hara, M. Sasaki and M. Inoue:
Relaxation Phenomena of Remanent Magnetizations in Spin- and Cluster-Glasses of Itinerant Magnetic Fe_xTiS_2 Crystals Studied by Hall Effect,
J. Phys. Chem. Solids (1996) (in press).